This is a preprint, the final version is subject to change, of the American Mineralogist (MSA)
Cite as Authors (Year) Title. American Mineralogist, in press.
(DOI will not work until issue is live.) DOI: http://dx.doi.org/10.2138/am.2013.4438

Coexisting hydroxyl groups and H_2O molecules in minerals: A single-crystal neutron diffraction study of eosphorite, $MnAlPO_4(OH)_2 \cdot H_2O$

G. Diego Gatta[1], Gwilherm Nénert[2], Pietro Vignola[1,3]

[1] Dipartimento di Scienze della Terra, Universita' degli Studi di Milano,
Via Botticelli 23, I-20133 Milano, Italy
[2] Institut Laue-Langevin, BP 156, 38042 Grenoble Cedex 9, France
[3] CNR-Istituto per la Dinamica dei Processi Ambientali,
Via Mario Bianco 9, I-20131 Milano, Italy

Abstract

The crystal chemistry of eosphorite from Chamachhu (Skardu District, Baltistan, Pakistan) $[(Mn^{2+}_{0.94}Fe^{2+}_{0.06}Al_{0.01})_{\Sigma 1.01}AlPO_4(OH_{1.90}F_{0.10})_{\Sigma 2} \cdot H_2O$, a = 6.9263(4), b = 10.4356(8), c = 13.5234(10) Å, V = 977.5(1) Å^3, space group *Cmca, Z = 8*], has been reinvestigated by means of electron microprobe analysis in wavelength-dispersive mode and single-crystal neutron diffraction at 20 K. The anisotropic structural refinement has been performed with final agreement index R_1 = 0.0381 for 82 refined parameters and 860 unique reflections with $Fo > 4\sigma(Fo)$. The analysis of the difference-Fourier maps of the nuclear density allowed an unambiguous location of the H sites, and the description of the H_2O molecule and the OH groups configuration, along with the hydrogen bonding scheme. We can now describe the structure of eosphorite as made by $(Mn,Fe)O_4(OH,H_2O)_2$ and $AlO_2(OH)_2(OH,H_2O)_2$ octahedra, which both form chains running along [100]. The two types of chains are connected, via corner-sharing, to form a set of (100) sheets held together by P-tetrahedra (and hydrogen bonds) up to form a three-dimensional framework. This material provides the rare opportunity to investigate the H-bond configuration of coexisting hydroxyl groups and H_2O molecules in minerals by single-crystal neutron diffraction.

Key-words: eosphorite, crystal chemistry, single-crystal neutron diffraction, hydrogen bonding.

Introduction

Minerals belonging to the eosphorite [$MnAl(PO_4)(OH)_2 \cdot H_2O$] - childrenite [$FeAl(PO_4)(OH)_2 \bullet H_2O$] series, with the following ideal chemical formula $M^{2+}Al(PO_4)(OH)_2 \bullet H_2O$, where $M^{+} = Fe^{2+}$, Mn^{2+} (Hurlbut 1950, Fransolet 1980), are widespread secondary phosphates occurring in medium to strongly evolved rare-element granitic pegmatites ranging from the beryl- to the petalite-subtype in the classification of Černý and Ercit (2005). Eosphorite, in particular, is a low-temperature metasomatic mineral in Lithium-Cesium-Tantalum (LCT) granitic pegmatites, where it usually crystallizes in open cavities of pegmatitic dikes (Simmons et al. 2003). Eosphorite is one of the low-*T* alteration products of primary phosphates, mainly lithiophilite. It forms prismatic elongated crystals (up to 10 cm), frequently grouped in divergent clusters of pale-brown or pale-pinkish color.

The unit-cell constants and the possible space groups of childrenite (*Bbam* or *Bba*2) were first reported by Barnes (1949). The crystal structure of childrenite was later solved by Giuseppetti and Tadini (1984) by means of X-ray single-crystal diffraction. The authors refined the crystal structure in the acentric space group *Bba*2, with a = 10.395(1), b = 13.394(1), and c = 6.918(1) Å (Z = 8) (childrenite composition: $(Mn_{0.11}Fe_{0.89})Al(PO_4)(OH)_2 \bullet H_2O$].

The crystal-structure of eosphorite was first solved by Hanson (1960) in the centric *Bbam* space group, with $a \sim 10.52$, $b \sim 13.60$, and $c \sim 6.97$ Å (Z = 8), and later reinvestigated by Hoyos et al. (1993) by means of X-ray single-crystal diffraction, in the *Cmca* space group, with a = 6.928(1), b = 10.445(1), and c = 13.501(2) Å [eosphorite

83 composition: $(Mn_{0.76}Fe_{0.24})Al(PO_4)(OH)_2 \bullet H_2O]$. Hoyos et al. (1993) studied the optical
84 absorption and photoluminescence of the eosphorite sample used for the X-ray
85 investigation.

86 The crystal structure of both eosphorite and childrenite consists of chains
87 parallel to the *a*-axis (in the *Cmca* space group) constituted by (Mn,Fe)-distorted
88 octahedra, sharing opposite O-O edges, and chains of Al-octahedra. The two types of
89 chains are connected, via corner-sharing, to form a set of (100) sheets held together by
90 $[PO_4]$ tetrahedra (and hydrogen bonds) to form a three-dimensional network, as shown
91 in Fig. 1.

92 Despite the general structural model of Hoyos et al. (1993) for eosphorite being
93 correct, as shown by bond distances and angles, the quality of the X-ray diffraction data
94 at that time did not allow the authors to provide: 1) a non-ambiguous picture about the
95 Fe/Mn-ordering in the octahedral sites (assuming a fully disordered configuration with
96 one independent Fe/Mn-octahedral site), 2) the localization of all the proton sites,
97 leaving open questions concerning the topological configuration of the H_2O molecule
98 and of the OH-groups, their displacement regime along with the role played by the H-
99 bonds. The location of the proton sites and the nature of the H-bond in this material are
100 not secondary, as the total amount of H_2O is ~ 16 wt%. In addition, this material
101 provides the rare opportunity to investigate the different role played by H-bonds of
102 coexisting hydroxyl groups and H_2O molecules by single-crystal neutron diffraction. In
103 this light, the aim of the present study is a re-investigation of the crystal structure of a
104 natural eosphorite (with low Fe content) by means of low temperature single-crystal
105 neutron diffraction, in order to define: *a*) the location of the proton sites, and the real
106 topological configuration of the H_2O molecules and OH-groups, for a full description of
107 the inter-atomic relationship via H-bond; *b*) the anisotropic displacement parameters of

all the atomic sites, H included. The low-*T* data are useful to reduce thermal libration motion, which could be significant in this class of materials. Since the previous X-ray diffraction studies have proved to be insufficient to locate directly the H atoms, single-crystal neutron diffraction represents, therefore, the only experimental technique that allows to answer the open questions about the crystal structure of this hydrous phosphate.

Samples description and mineralogy

A single crystal of eosphorite up to 14 mm in length and 5 mm in diameter, coming from a granitic pegmatite outcropping in the area of Chamachhu (Changmachhu), Skardu district, Baltistan, Pakistan, was used both for this study. The sample comes from a pegmatitic dike located near the little village of Chamachhu, 10 km East of Shengus, along the Indus River on the Gilgit-Skardu road (Blauwet et al. 1997, Kazmi et al. 1985). Eosphorite from Chamachhu occurs as crystals perched on white platy albite (cleavelandite) or on large pollucite crystals (up to 20-30 cm) contained in large miarolitic cavities. The mineralogical association of these pegmatites is fairly evolved and represented by muscovite, lepidolite, spessartine, elbaite, topaz, beryl (gem aquamarine and morganite), pollucite, tantalite-(Mn), fluorapatite, eosphorite, and väyrynenite. The pegmatitic field is hosted by metamorphic rocks belonging to the Nanga Parbat-Haramosh Massif (Searle 1991).

Experimental methods

A prismatic, 14 mm long single-crystal of eosphorite was cut in several fragments used for the chemical analysis and for the neutron diffraction experiment.

Quantitative electron microprobe analysis in wavelength-dispersive mode (EPMA-WDS) was performed on a polished fragment (1.1 x 0.8 x 0.3 mm^3) of the original crystal of eosphorite using a Jeol JXA-8200 electron microprobe at the Earth Science Department of the University of Milano, Italy. The system was operated with an accelerating voltage of 15 kV, a beam current of 5 nA, a counting time of 30 s on the peaks and 10 s on the backgrounds, and a beam diameter of 5 μm. Minerals (graftonite for P, Fe, Mn and Ca, grossular for Si and Al, K-feldspar for K, forsterite for Mg, omphacite for Na, cancrinite for Cl, and hornblende for F) were used as standards. The raw data were corrected for matrix effects using the ΦρZ method as implemented in the JEOL suite of programs. The average chemical composition and the proportional formula of the investigated eosphorite are given in Table 1.

A second fragment (3.2 x 3.5 x 4.5 mm, Table 2) of the original crystal of eosphorite, free of defect or twinning under the polarised microscope, was used for the neutron diffraction experiment. A preliminary characterization of the single crystal was performed using the Laue backscattering technique as available on the instrument Orient-Express at the Institut Laue-Langevin (ILL), Grenoble (Ouladdiaf et al. 2006). The sample presented broad reflections spots. Consequently, broad scans in omega (up to 6°) were performed for the data collection in order to get the whole integrated intensities. Intensity data were collected at 20 K on the high resolution four-circle diffractometer D9 at ILL using a wavelength of 0.8390(1) Å obtained by reflection from a Cu(220) monochromator. The wavelength was calibrated using a germanium single crystal. D9 is equipped with a small two-dimensional area detector (Lehmann et al. 1989), which for this measurement allowed optimal delineation of the peak from the background. A total number of 2451 reflections (of the type $\pm h$, $\pm k$, $\pm l$) were collected up to $2\theta_{max}$ = 91.1°, giving rise to 873 unique reflections (Table 2). For all data,

157 background corrections following Wilkinson et al. (1988) and Lorentz corrections were
158 applied. After corrections, the discrepancy factors among the symmetry related
159 reflections was R_{int} = 0.0330 (Laue class *mmm*) (Table 2).

160 Least-squares matching of the observed and calculated centroids of the 1078
161 strongest reflections gave a metrically orthorhombic unit cell with: a = 6.9263(4), b =
162 10.4356(8), and c = 13.5234(10) Å, with a *C*-centered lattice. Other details pertaining to
163 the data collections are listed in Table 2.

164 A careful inspection of the diffraction intensities did not show any significant
165 evidence of magnetic ordering in eosphorite structure at 20 K.

166

167 **Structure refinements**

168 The neutron diffraction data of eosphorite were first processed with the program
169 E-STATISTICS, implemented in the WinGX package (Farrugia 1999). The Wilson plot
170 was carried out and the normalized structure factors (*E*'s) and their statistics of
171 distributions were calculated. The structure of eosphorite was found to be
172 centrosymmetric at 92.9 % likelihood. A similar result was obtained by the Sheldrick's
173 $|E^2\text{-}1|$ criterion (Sheldrick 1997), with $|E^2\text{-}1| = 0.962$. On the basis of the reflections
174 conditions and of the presence of the inversion center, the crystal structure refinement
175 was then performed in the space group *Cmca* using the SHELX-97 software (Sheldrick
176 1997), with anisotropic thermal displacement parameters. The starting model was that
177 of Hoyos et al. (1993), without any H site. The neutron scattering lengths of Mn, Fe, Al,
178 P, O, F and H have been used according to the Sears (1986). The secondary isotropic
179 extinction effect was corrected according to Larson's formalism (1967), as implemented
180 in the SHELXL-97 package (Sheldrick 1997). The octahedral *M* site was modeled with
181 the scattering lengths of Mn and Fe, and the occupancy of the two elements was refined

(Table 3). When convergence was achieved, three intense negative residual peaks were found in the final difference-Fourier map of the nuclear density. Further refinement cycles were then performed assigning H to these residual peaks (*i.e. H1*, *H2* and *H3* site, Fig. 2, Table 3), as hydrogen has a negative neutron scattering length (Sears 1986). The final least-square cycles were conducted with anisotropic thermal parameters for all sites including the H-sites. A mixed scattering length of O and F was used to model the *O3* and *O4* sites. However, this did not improve the figures of merit of the refinement, leading to a not significant site occupancy factor of fluorine. When convergence was achieved, all the principal mean-square atomic displacement parameters were positively defined and the variance-covariance matrix showed no significant correlation among the refined parameters (*i.e.* no correlation higher than 0.5). At the end of the last cycle of refinement, no peak larger than +0.6/-0.6 fm/Å^3 was present in the final difference-Fourier map of the nuclear density (Table 2). The final agreement index (R_1) was 0.0381 for 82 refined parameters and 860 unique reflections with Fo>4σ(Fo) (Table 2). Atomic positions and displacement parameters (U_{ij}) are reported in Table 3. Principal root-mean-square components of the atomic displacements parameters are given in Table 4. Bond lengths and angles are listed in Tables 5.

A further test refinement of the structure of eosphorite was performed in the acentric space group *C*2*cb*. In this case, four independent H sites were located. The refinement converged to the final agreement index R_1 = 0.0314 (for *n. obs. unique reflect.* / *n. ref. parameters* = 9.7), with no residuals larger than +0.6/-0.5 fm/Å^3. However, when convergence was achieved, the principal mean-square atomic displacement parameters of the (Mn,Fe) site were not positively defined and several other displacement ellipsoids showed a drastically high, and unacceptable, anisotropy.

206 In addition, the variance-covariance matrix showed significant correlations (> 0.82)
207 among the refined parameters.
208
209 **Discussion and Conclusions**
210 The single-crystal neutron structure refinement of this study provides a general
211 structure model in agreement with the previous one reported by Hoyos et al. (1993). The
212 statistics of distributions of the normalized structure factors (*E*'s) and the Wilson plot
213 suggested that the structure is centrosymmetric. This result is corroborates by the
214 structure refinements performed in the space groups *Cmca* and *C*2*cb*. Our experimental
215 findings confirm the previous results reported by Hoyos et al. (1993), who performed a
216 piezoelectricity test on a crystal of eosphorite (from Taquaral, Brazil) showing no
217 evidence of activity in the frequency range from 100 to 1000 KHz, so suggesting the
218 presence of a centre of symmetry.
219 The building block units of the eosphorite structure consist of chains of (Mn,Fe)-
220 octahedra (sharing opposite O-O edges) running along the *a*-axis, and chains of Al-
221 octahedra. The two types of chains are connected, via corner-sharing, to form a set of
222 (100) sheets held together by P-tetrahedra (and hydrogen bonds) to form a three-
223 dimensional framework, as shown in Fig. 1. Distorted channels, confined by a 6-
224 membered ring of polyhedra, run along [100]. The (Mn,Fe)-octahedron is significantly
225 distorted, with $\Delta(\text{O-O})_{max}$ ~ 0.81 Å (*i.e.,* the difference between the longest and the
226 shortest O-O distances) (Table 5), the O-O distance of the shared-edge being
227 significantly shorter than the non-shared ones. We cannot exclude that this is the effect
228 due to the cation-cation repulsion, as *M*-*M* ~ 3.46 Å. The Al-octahedron and the P-
229 tetrahedron appear to be less distorted, with $\Delta(\text{O-O})_{max}$ ~ 0.15 Å and $\Delta(\text{O-O})_{max}$ ~ 0.03
230 Å, respectively (Table 5).

The low-*T* structure refinement does not show any evidence of (Mn,Fe)-octahedral ordering, which should lead to a lowering of the symmetry. In addition, the principal root-mean-square components of the atomic displacements parameters (Table 4) do not show any pronounced displacement about the equilibrium position, if compared with those of the other atomic sites, suggesting the absence of a local site splitting. The Fe-content deduced on the basis of the structure refinement is 0.056(1) *a.p.f.u*. (Table 3), in good agreement with the chemical analysis (*i.e.* Fe 0.061 *a.p.f.u*., Table 1). The EPMA-WDS data shows a slight excess of Al (about 0.01 *a.p.f.u*., Table 1), as often reported in eosphorite (*e.g.,* samples from Black Mountain, Maine, and Buckfield, Maine; Hurlbut 1950).

The neutron structure refinement of this study allowed an unambiguous location of the H-sites along with the description of the H-bonding scheme in eosphorite structure. We can now describe the structure as made by $(Mn,Fe)O_4(OH,H_2O)_2$ and $AlO_2(OH)_2(OH,H_2O)_2$ octahedra (Figs. 1 and 2). The *O3* site is the OH-group (*i.e., O3-H3*) oxygen, whereas *O4* is the oxygen of OH-group (*i.e., O4-H1*) and H_2O molecules (*i.e., H2-O4-H1*) (Figs. 1 and 2, Table 5). In particular, H_2O molecules have site occupancy of 50%, so that the two H_2O molecules generated by the mirror plane are mutually exclusive (Fig. 2, Table 3). In other words, the two equivalent *O4* sites generated by the mirror plane are respectively the oxygen of one OH group and one H_2O molecule, with a local breaking of the symmetry, as shown in Fig. 2. Among the three independent Al-O bond distances of the $AlO_2(OH)_2(OH,H_2O)_2$ octahedron, the Al-OH bond distance (*i.e.,* Al-O3) is the shortest and the Al-(OH,H_2O) distance (*i.e.,* Al-O4) the longest, respectively (Table 5). In the $(Mn,Fe)O_4(OH,H_2O)_2$ polyhedron, the *M*-$(OH,H_2O)_2$ bond distance (*i.e. M-O4*) is the longest (Table 5).

The location of the H sites and the configuration of the OH group and H_2O molecules suggested by Hoyos et al. (1993), on the basis of X-ray diffraction data, were not correct: the *O3* site was considered as H_2O oxygen atom, whereas the *O4* site as OH group atom.

The geometry of the H_2O molecule and the OH group, along with the hydrogen bonding scheme in eosphorite, are now well defined. The *O4-H1* and *O4-H2* distances, corrected for "riding motion" (Busing and Levy 1964), are ~1.003 and ~1.071 Å, respectively (Table 5), and two strong hydrogen bonds energetically favorable occur: *O4···O5* = 2.711(1) Å, *H1···O5* = 1.757(1) Å and *O4-H1···O5* = 161.9(1)°; *O4···O4* = 2.504(1) Å, *H2···O4* = 1.454(1) Å and *O4-H1···O4* = 170.9(1)° (Fig. 2, Table 5). In other words, symmetry-related *O4* act as *donor* and as *acceptor* of the H-bond. The *H1-O4-H2* angle approaches the ideal value (*i.e.,* 107.2(1); Fig. 2, Table 5) (Chiari and Ferraris 1982, Steiner 1998, Gatta et al. 2008, 2009, 2012). The OH-group shows: *O3-H3* distance, corrected for "riding motion", of ~ 0.995 Å, *O3···O1* = 2.836(1) Å, *H3···O1* = 1.930(1) Å and *O3-H3···O1* = 154.0(1)° (Fig. 2, Table 5). The *O1* site (*i.e.* the *acceptor* of the H bond of the *O3-H3* group) is *underbonded*, as it is shared by two (Mn,Fe)-octahedra and one P-tetrahedra (Fig. 2, Table 5).

The anisotropic structure refinement shows that the principal root-mean-square components of the atomic displacements parameters of the *H3* site (belonging to the OH group) are larger in magnitude than those of the *H1* and *H2* sites (belonging to the H_2O molecules, Table 4).

Acknowledgments

The authors thank the Institut Laue-Langevin, Grenoble, France, for the allocation of neutron beam time. The authors are grateful to E. Marini for the eosphorite sample, and to F. Pezzotta for the fruitful discussion. A. Locock, an anonymous reviewer and the Associate Editor H. Xu are thanked for the revision of the manuscript. This study was founded by the Italian Ministry of University and Research, MIUR-Project: 2010EARRRZ_003.

References

Barnes, W.H. (1949) The unit cell and space group of childrenite. American Mineralogist, 34, 12-18.

Blauwet, D., Smith, B., and Smith, C. (1997) A guide to the mineral localities of the Northern Areas, Pakistan. Mineralogical Record, 28, 3, 183-200.

Busing W.R. and Levy H.A. (1964) The effect of thermal motion on the estimation of bond lengths from diffraction measurements. Acta Crystallographica, 17, 142-146.

Černý, P. and Ercit, S. (2005): The classification of granitic pegmatites revisited. Canadian Mineralogist, 43, 2005-2026.

Chiari, G. and Ferraris, G. (1982) The water molecules in crystalline hydrates studied by neutron diffraction. Acta Crystallographica, B38, 2331-2341.

Farrugia, L.J. (1999) WinGX suite for small-molecule single-crystal crystallography. Journal of Applied Crystallography, 32, 837-838.

Fransolet, A.M. (1980) The eosphorite-childrenite series associated with the Li-Mn-Fe phosphate minerals from the Buranga Pegmatite, Rwanda. Mineralogical Magazine, 43, 1015-1023.

306 Gatta, G.D., Rotiroti, N., McIntyre, G.J., Guastoni, A., and Nestola F. (2008) New
307 insights into the crystal chemistry of epididymite and eudidymite from Malosa, Malawi:
308 a single-crystal neutron diffraction study. American Mineralogist, 93, 1158-1165.
309 Gatta, G.D., Rinaldi, R., McIntyre, G.J., Nénert, G., Bellatreccia, F., Guastoni, A.,
310 and Della Ventura G. (2009) On the crystal structure and crystal chemistry of pollucite,
311 $(Cs,Na)_{16}Al_{16}Si_{32}O_{96}{\cdot}nH_2O$: a natural microporous material of interest in nuclear
312 technology. American Mineralogist, 94, 1560-1568.
313 Gatta, G.D., McIntyre, G.J., Swanson, G.J., and Jacobsen, S.D. (2012) Minerals in
314 cement chemistry: a single-crystal neutron diffraction and Raman spectroscopic study of
315 thaumasite, $Ca_3Si(OH)_6(CO_3)(SO_4){\bullet}12H_2O$. American Mineralogist, 97, 1060–1069.
316 Giuseppetti, G., and Tadini, C. (1986) The crystal structure of childrenite from
317 Tavistock (SW England), $Ch_{89}E0_{11}$ term of childrenite-eosphorite series. Neues
318 Jahrbuch für Mineralogie Monatshefte, 263-271.
319 Hanson, A.W. (1960) The crystal ctructure of eosphorite. Acta Crystallographica,
320 13, 384-387.
321 Hoyos, M.A., Calderon, T., Vergara, I., and Garcia-Solé, J. (1993) New structure
322 and spectroscopic data for eosphorite. Mineralogical Magazine, 57, 329-336.
323 Hurlbut, C. (1950) Childrenite-eosphorite series. American Mineralogist, 35, 793–
324 805.
325 Kazmi, A.H., Peters, J.J., and Obodda, H.P. (1985) Gem pegmatites of the
326 Shengus-Dusso area, Gilgit, Pakistan. Mineralogical Record, 16, 5, 393-411.
327 Larson, A.C. (1967) Inclusion of secondary extinction in least-squares
328 calculations. Acta Crystallographica, 23, 664 – 665.

Lehmann, M. S., Kuhs, W., McIntyre, G.J., Wilkinson, C., and Allibon, J. (1989) On the use of a small two-dimensional position-sensitive detector in neutron diffraction. Journal of Applied Crystallography, 22, 562-568.

Ouladdiaf, B., Archer, J., McIntyre, G.J., Hewat, A.W., Brau, D., and York, S. (2006) OrientExpress: A new system for Laue neutron diffraction. Physica B, 385-386, 1052-1054.

Searle, M.P. (1991) Geology and Tectonics of the Karakoram Mountains. John Wiley & Sons, Chichester, United Kingdom, 358 pp..

Sears, V.F. (1986) Neutron Scattering Lengths and Cross-Sections. In K. Sköld and D.L. Price, Eds., Neutron Scattering, Methods of Experimental Physics, Vol. 23A, p. 521-550. Academic Press, New York.

Sheldrick, G.M. (1997) SHELX-97. Programs for crystal structure determination and refinement. University of Göttingen, Germany.

Simmons, W., Webber, K.L., Falster, A.U., and Nizamoff, J.W. (2003) Pegmatology – Pegmatite Mineralogy, Petrology and Petrogenesis. Rubellite Press, New Orleans, Louisiana, 176 pp..

Steiner, T. (1998) Opening and narrowing of the water H-O-H angle by hydrogen-bonding effects: Re-inspection of neutron diffraction data. Acta Crystallographica, B54, 464-470.

Wilkinson, C., Khamis, H.W., Stansfield, R.F.D., and McIntyre, G.J. (1988) Integration of single-crystal reflections using area multidetectors. Journal of Applied Crystallography, 21, 471-478.

Table and Figure captions

Table 1. Averaged (22 points) WDS electron-microprobe analysis of eosphorite from Chamachhu.

Table 2. Details of neutron data collection and refinement of eosphorite.

Table 3. Refined positional and thermal displacement parameters ($Å^2$) and site occupancy factors of eosphorite. The anisotropic displacement factor exponent takes the form: $-2\pi^2[(ha^*)^2U_{11} + \ldots + 2hka^*b^*U_{12}]$. U_{eq} is defined as one third of the trace of the orthogonalised U_{ij} tensor.

Table 4. Principal root-mean-square components (R1, R2 and R3, x 10^2 Å) of the atomic displacements parameters.

Table 5. Relevant bond distances (Å) and angles (°) in the eosphorite structure.

Fig. 1. (*Above*) The crystal structure of eosphorite viewed down [100], based on the neutron structure refinement of this study at 20 K. Thermal ellipsoid probability factor: 50%. (Mn,Fe) octahedra are in dark grey, Al octahedra in light grey, P tetrahedra in light grey. (*Below*) Clinographic view of the structure. The building block units of the eosphorite structure consists of chains of (Mn,Fe)-octahedra (sharing opposite O-O edges) running along the *a*-axis, and chains of Al-octahedra. The two types of chains are connected, via corner-sharing, to form a set of (100) sheets held together by P-tetrahedra (and hydrogen bonds) up to form a three-dimensional framework.

Fig. 2. Hydrogen location, configuration of OH groups and H_2O molecules, along with H-bond scheme, in the structure of eosphorite. The occupancy factor of the H2 site is 50%.

Table 1. Averaged (22 points) WDS electron-microprobe analysis of eosphorite from Chamachhu.

	wt%	*e.s.d.*		*a.p.f.u.*
P_2O_5	30.98	0.21	P	1.000
Al_2O_3	22.56	0.07	Al	1.009
FeO	1.92	0.20	Fe^{2+}	0.061
MnO	29.12	0.10	Mn^{2+}	0.940
MgO	0.04	0.02	Mg	0.002
CaO	0.09	0.07	Ca	0.004
Na_2O	0.08	0.01	Na	0.006
*H_2O	14.90		OH^-	1.897
*F	0.86	0.12	F^-	0.103
sum	100.56			
O=F	-0.36		H_2O	1.000
TOTAL	100.20			

Notes: Si, As, K and Cl were below detection limit; formula proportions calculated on the basis of 1 atom of P per formula unit (*a.p.f.u.*); *calculated considering (OH+F) = 2 *a.p.f.u.* and H_2O = 1 molecule *p.f.u.*.

Table 2. Details of neutron data collection and refinement of eosphorite.

Crystal shape	Prismatic
Crystal size (mm)	3.2 x 3.5 x 4.5
Crystal color	Translucent pink
Unit-cell constants	a = 6.9263(4) Å
	b = 10.4356(8) Å
	c = 13.5234(10) Å
	V = 977.5(1) Å^3
Chemical formula	$MnAl(PO_4)(OH)_2 \bullet H_2O$
Space Group	*Cmca*
Z	8
T (K)	20
Radiation (Å)	0.8390(1)
Diffractometer	D9 four circle
Data-collection method	ω-θ scans
Max. 2θ(°)	91.1
	$-11 \le h \le 8$
	$-11 \le k \le 14$
	$-7 \le l \le 20$
No. measured reflections	2451
No. unique reflections	873
No. unique refl. with $F_o > 4\sigma(F_o)$	860
No. refined parameters	82
R_{int}	0.0330
R_1 (F) with $F_o > 4\sigma(F_o)$	0.0381
R_1 (F) for all the unique refl.	0.0394
wR_2 (F^2)	0.0689
S	3.240
Weighting Scheme: a, b	0.01, 0
Residuals (fm/ Å^3)	+0.6/-0.6

Note: $R_{int} = \Sigma|F_{obs}^2 - F_{obs}^2(mean)|/\Sigma[F_{obs}^2]$; $R_1 = \Sigma(|F_{obs}| - |F_{calc}|)/\Sigma|F_{obs}|$; $wR_2 = [\Sigma[w(F^2_{obs} - F^2_{calc})^2]/\Sigma[w(F^2_{obs})^2]]^{0.5}$, $w = 1/[\sigma^2(F_{obs}^2) + (a*P)^2 + b*P]$, $P = (\text{Max}(F_{obs}^2, 0) + 2*F_{calc}^2)/3$

Table 3. Refined positional and thermal displacement parameters (Å^2) and site occupancy factors of eosphorite. The anisotropic displacement factor exponent takes the form: $-2\pi^2[(ha^*)^2U_{11} + \ldots + 2hka^*b^*U_{12}]$. U_{eq} is defined as one third of the trace of the orthogonalized U_{ij} tensor.

Site	*s.o.f.*	*x/a*	*y/b*	*z/c*	U_{11}	U_{22}	U_{33}	U_{12}	U_{13}	U_{23}	U_{eq}
M	Mn, 0.944(1) Fe, 0.056(1)	0.25	0.13423(14)	0.25	0.0032(3)	0.0055(6)	0.0103(6)	0	-0.0015(3)	0	0.0063(2)
Al	Al, 1	0.25	0.25	0	0.0033(2)	0.0091(5)	0.0066(5)	-0.0012(3)	0.0009(2)	-0.0029(4)	0.0064(2)
P	P, 1	0	0.37739(8)	0.33377(5)	0.0033(2)	0.0061(3)	0.0056(3)	0	0	0.0008(3)	0.0050(1)
O1	O, 1	0	0.26580(7)	0.25871(5)	0.0071(2)	0.0063(3)	0.0058(3)	0	0	-0.0007(2)	0.0064(1)
O2	O, 1	0	0.00716(7)	0.21941(5)	0.0051(2)	0.0059(3)	0.0062(3)	0	0	-.0011(2)	0.0057(1)
O3	O, 1	0	0.25178(7)	0.04931(5)	0.0037(2)	0.0076(3)	0.0065(3)	0	0	0.0004(2)	0.0059(1)
O4	O, 1	0.18076(5)	0.11057(5)	0.40962(3)	0.0052(1)	0.0069(2)	0.0069(2)	0.0004(1)	-0.0001(1)	-0.0002(2)	0.0063(1)
O5	O, 1	0.31912(5)	0.13209(5)	0.60046(3)	0.0043(1)	0.0076(2)	0.0065(2)	0.0003(1)	-0.0005(1)	0.0013(2)	0.0061(1)
H1	H, 0.990(3)	0.23517(12)	0.02445(11)	0.42046(8)	0.0213(3)	0.0139(5)	0.0225(5)	0.0046(3)	-0.0007(3)	0.0023(4)	0.0192(2)
H2	H, 0.507(3)	0.02866(17)	0.10127(19)	0.41045(13)	0.009(1)	0.020(1)	0.021(1)	-0.002(0)	0	-0.001(1)	0.0165(5)
H3	H, 1	0	0.28409(18)	0.11668(11)	0.0181(4)	0.0349(9)	0.0176(6)	0	0	-0.0073(6)	0.0235(4)

Table 4. Principal root-mean-square components (R1, R2 and R3, x 10^2 Å) of the atomic displacements parameters.

Site	**R1**	**R2**	**R3**	**R1-R3**
M	10.2(2)	7.4(4)	5.4(3)	1.90
Al	10.6(2)	6.9(4)	5.5(2)	1.94
P	8.1(2)	7.1(2)	5.7(2)	1.41
O1	8.4(1)	8.2(2)	7.3(2)	1.14
O2	8.4(2)	7.1(1)	7.1(2)	1.19
O3	8.8(2)	7.9(2)	6.1(1)	1.44
O4	8.5(1)	8.2(1)	7.1(1)	1.19
O5	9.2(1)	7.6(1)	6.4(1)	1.44
H1	15.4(1)	15.1(2)	10.6(2)	1.45
H2	14.5(3)	14.0(3)	9.4(6)	1.53
H3	19.4(2)	13.4(1)	12.2(3)	1.59

Table 5. Relevant bond distances (Å) and angles (°) in the eosphorite structure.

M-O1 (x 2)	2.213(1)	*O4-H1*	0.985(1)
M-O2 (x 2)	2.220(1)	*O4-H1**	1.003
M-O4 (x 2)	2.2249(5)	*H1···O5*	1.757(1)
O1-O1	3.471(1)	*O4···O5*	2.711(1)
O1-O2	2.751(2)	*O4-H1···O5*	161.9(1)
O1-O4	2.8908(8)	*O4-H2*	1.058(1)
O1-O4'	3.563(1)	*O4-H2**	1.077
O2-O2	3.561(1)	*O4···O4*	2.504(1)
O2-O4	3.0163(6)	*H2···O4*	1.454(1)
O2-O4'	3.0576(8)	*O4-H1···O4*	170.9(1)
Al-O3 (x 2)	1.8556(3)	*H1-O4-H2*	107.2(1)
Al-O4 (x 2)	1.9599(5)	*O3-H3*	0.972(2)
Al-O5 (x 2)	1.8945(5)	*O3-H3**	0.995
O3-O4	2.683(1)	*O3···O1*	2.846(3)
O3-O4'	2.715(1)	*H3···O1*	1.930(1)
O3-O5	2.614(1)	*O3-H3···O1*	154.0(1)
O3-O5'	2.689(1)		
O4-O5	2.689(1)	*H2↔H2*	0.397(2)
O4-O5'	2.762(1)		
P-O1	1.545(1)		
P-O2	1.533(1)		
P-O5 (x 2)	1.5396(6)		
O1-O2	2.536(2)		
O1-O5	2.5164(8)		
O2-O5	2.5037(7)		
O5-O5	2.5057(8)		

* Bond distance corrected for "riding motion" following Busing and Levy (1964).

Fig. 1. (*Above*) The crystal structure of eosphorite viewed down [100], based on the neutron structure refinement of this study at 20 K. Thermal ellipsoid probability factor: 50%. (Mn,Fe) octahedra are in dark grey, Al octahedra in light grey, P tetrahedra in light grey. (*Below*) Clinographic view of the structure. The building block units of the eosphorite structure consists of chains of (Mn,Fe)-octahedra (sharing opposite O-O edges) running along the *a*-axis, and chains of Al-octahedra. The two types of chains are connected, via corner-sharing, to form a set of (100) sheets held together by P-tetrahedra (and hydrogen bonds) up to form a three-dimensional framework.

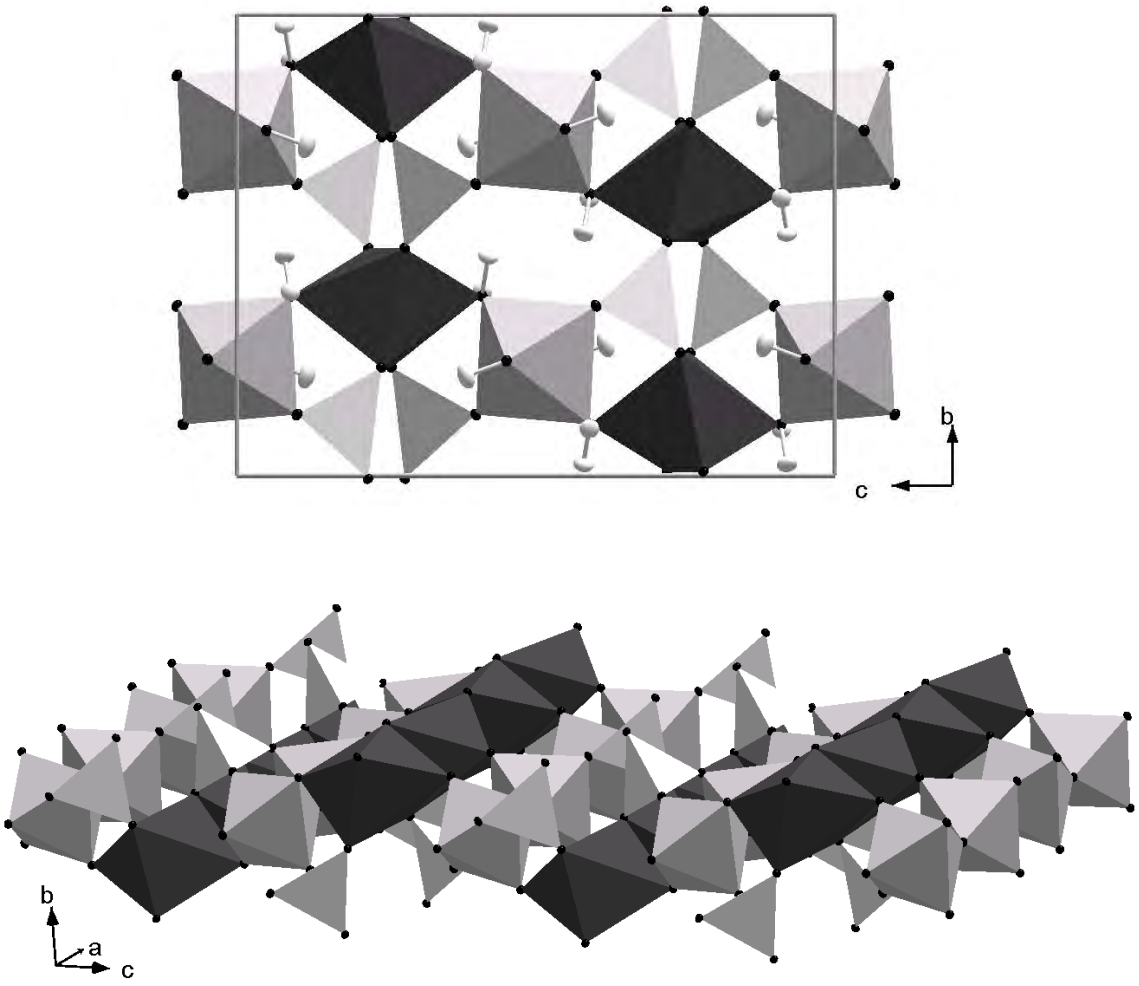

Fig. 2. Hydrogen location, configuration of OH groups and H_2O molecules, along with H-bond scheme, in the structure of eosphorite. The occupancy factor of the *H2* site is 50%.

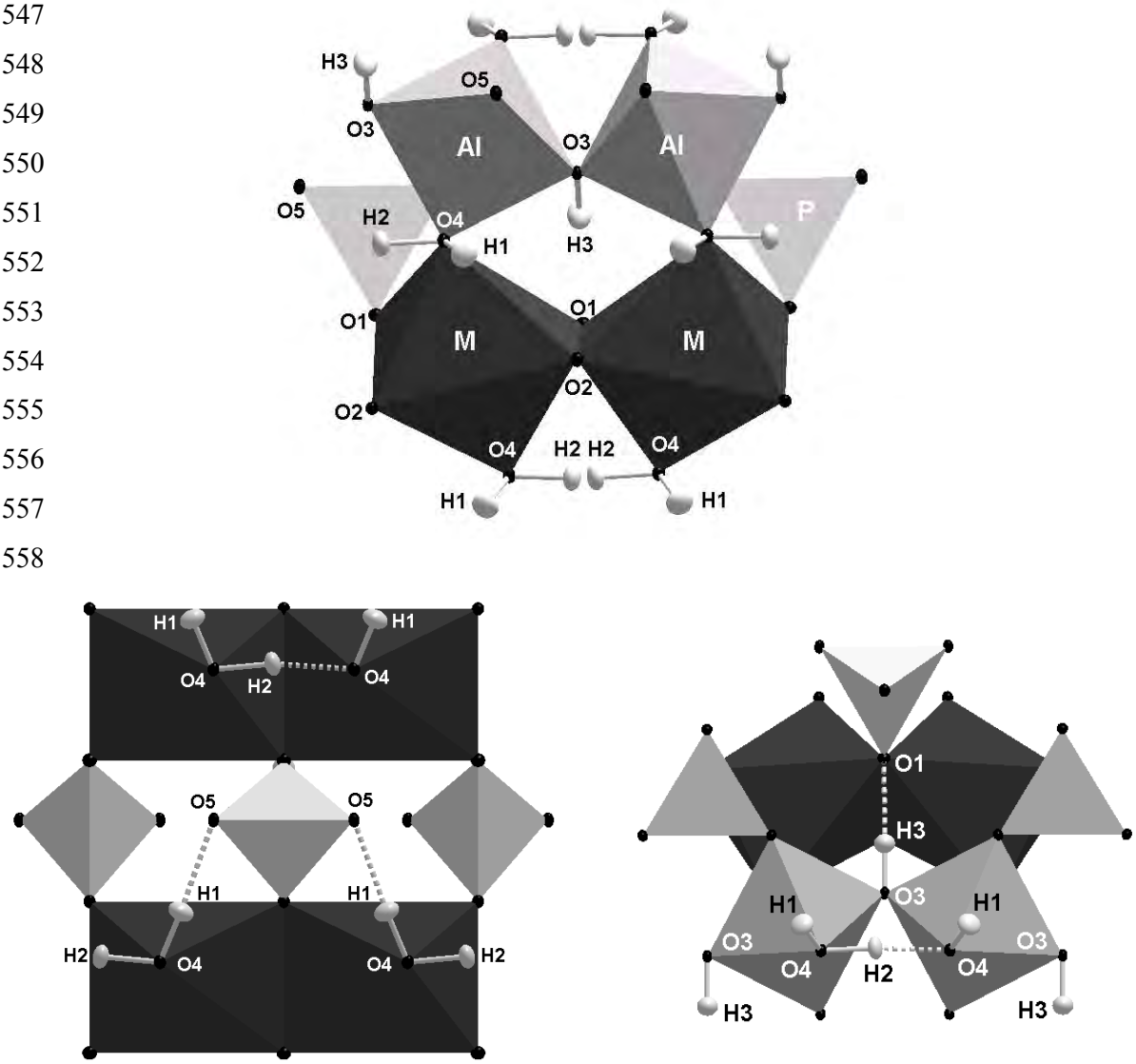

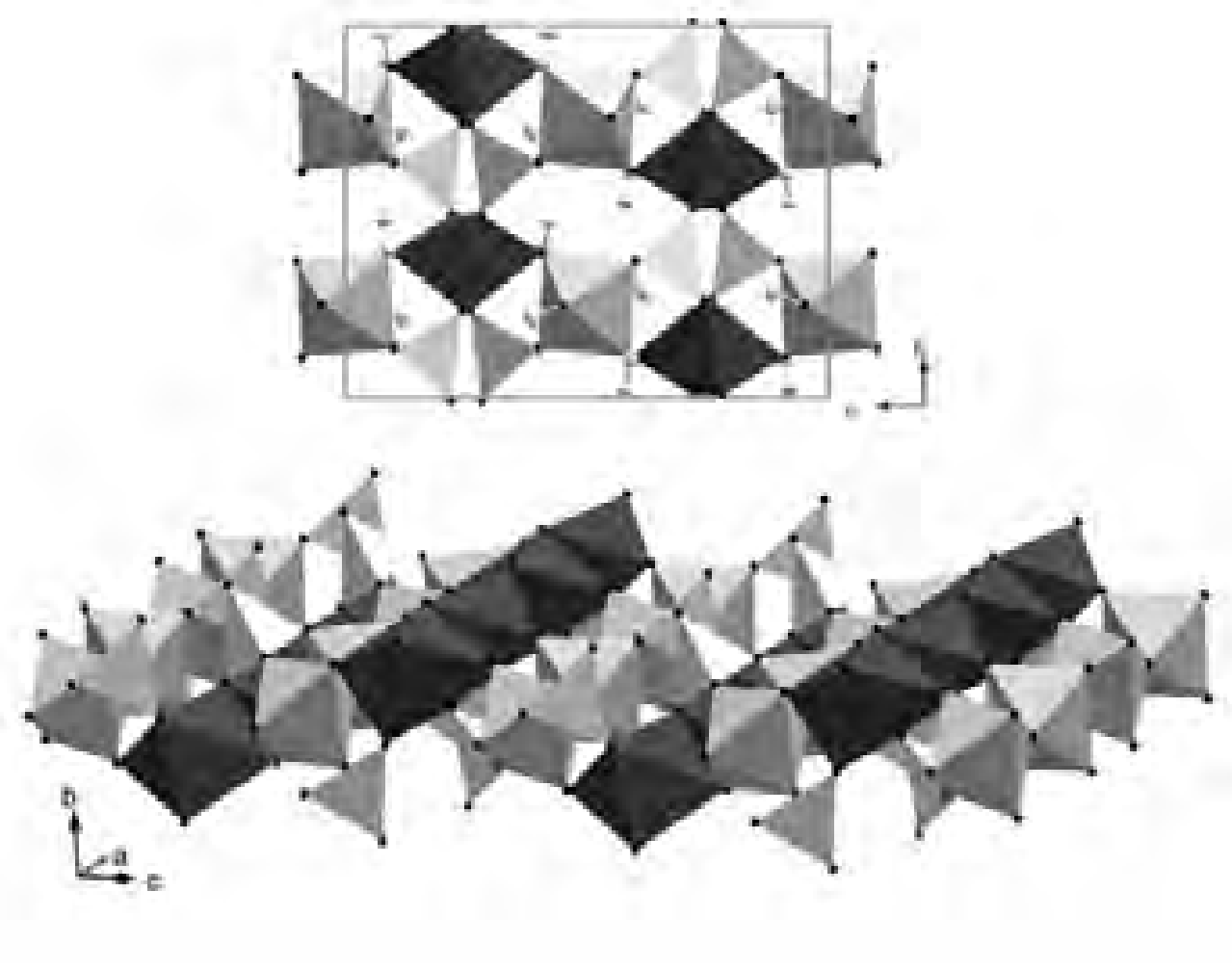
b
a
c

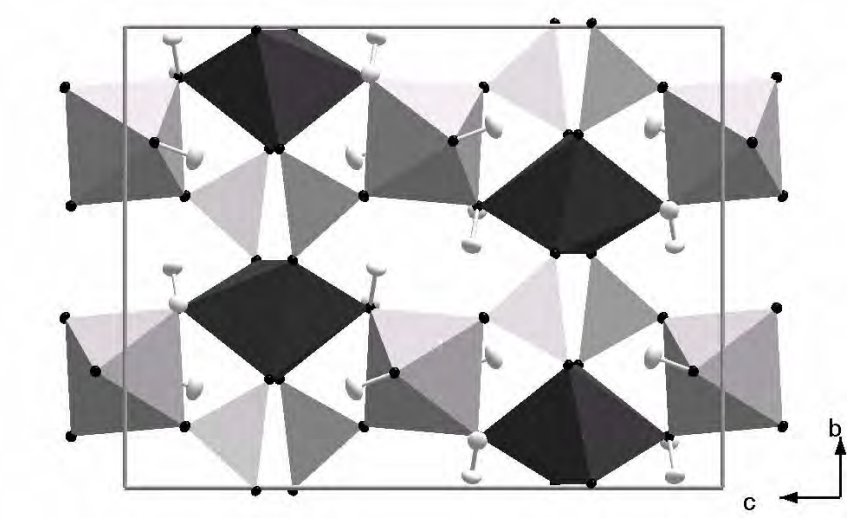
b
c

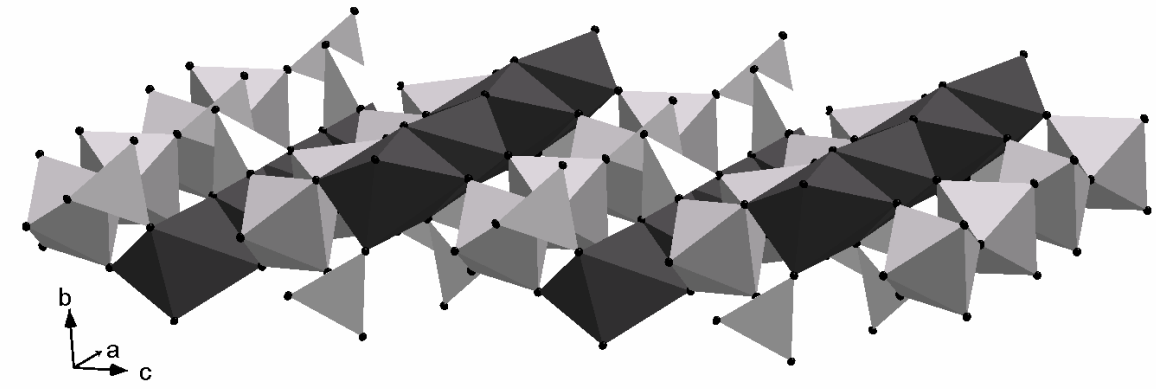
b
a
c

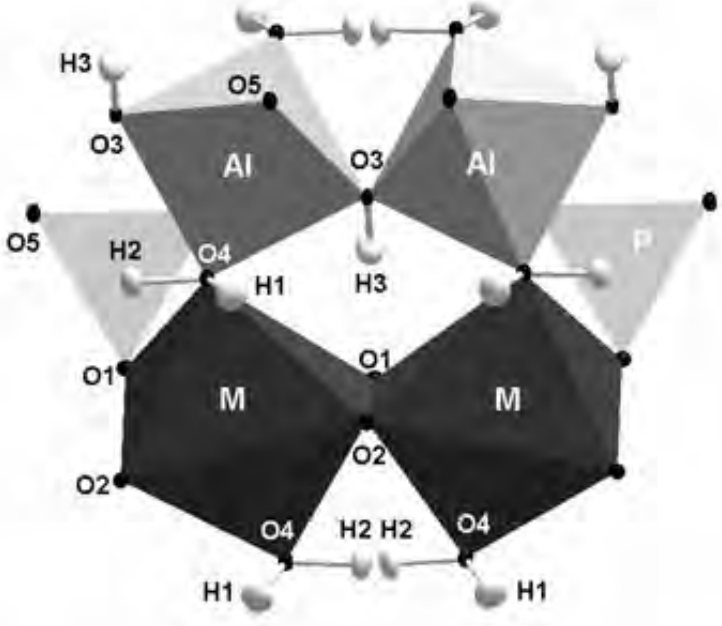
H3
O5
O3
Al
O3
Al
O5
H2
O4
H1
H3
P
O1
O1
M
M
O2
O2
O4
H2 H2
O4
H1
H1

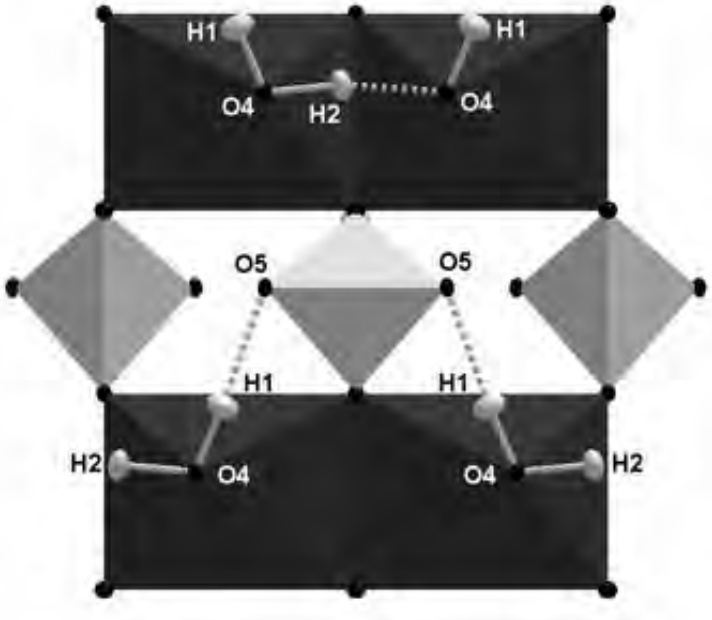
H1
H1
O4
H2
O4
O5
O5
H1
H1
H2
O4
O4
H2

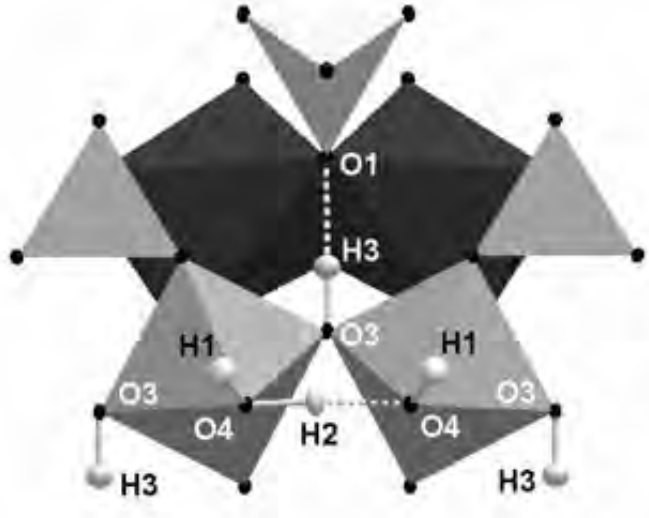
O1
H3
H1
O3
H1
O3
O3
O4
H2
O4
H3
H3

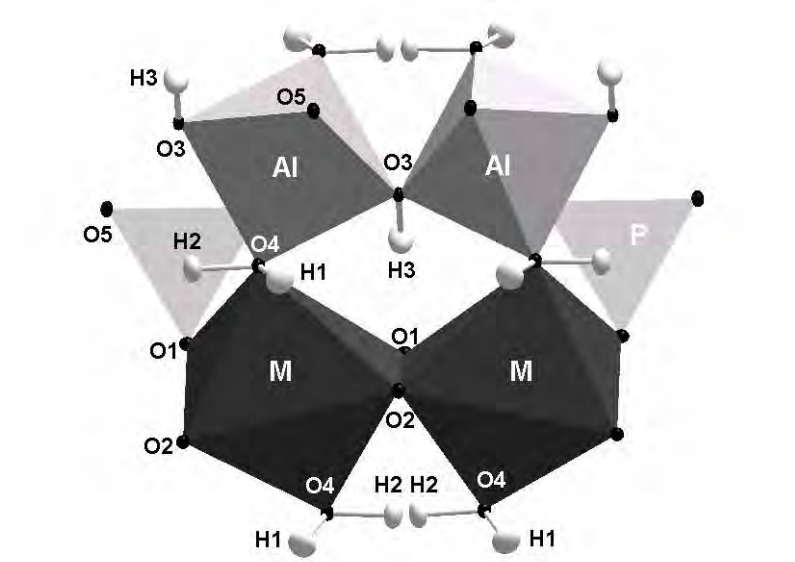
H3
O5
O3
Al
O3
Al
O5
H2
O4
H1
H3
P
O1
O1
M
M
O2
O2
O4
H2 H2
O4
H1
H1

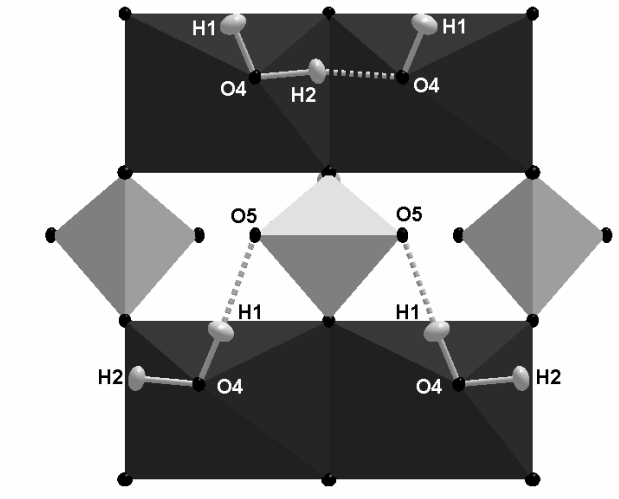
H1
H1
O4
H2
O4
O5
O5
H1
H1
H2
O4
O4
H2

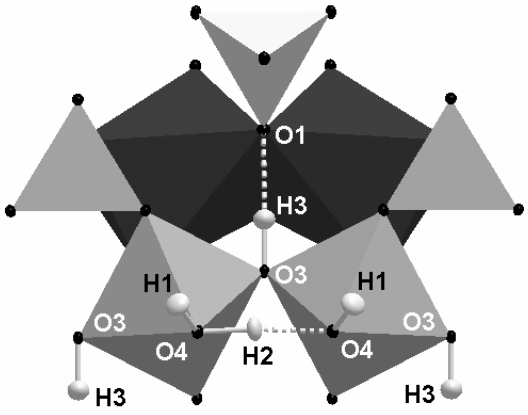
O1
H3
H1
O3
H1
O3
O3
O4
H2
O4
H3
H3